Seasonal variations in the lightning diurnal cycle and implications for the global electric circuit

Richard J. Blakeslee [a,*], Douglas M. Mach [b], Monte G. Bateman [c], Jeffrey C. Bailey [d]

[a] NASA Marshall Space Flight Center, Huntsville, AL 35812, USA
[b] University of Alabama in Huntsville, Huntsville, AL 35899, USA
[c] Universities Space Research Association, Huntsville, AL 35803, USA
[d] University of Alabama in Huntsville, Huntsville, AL 35899, USA

ARTICLE INFO

ABSTRACT

Data obtained from the Optical Transient Detector and the Lightning Imaging Sensor satellites (70° and 35° inclination low earth orbits, respectively) are used to statistically determine the number of flashes in the seasonal diurnal cycle as a function of local and universal time. These data include corrections for detection efficiency and instrument view time. They are further subdivided by season, land versus ocean, and other spatial (e.g., continents) and temporal (e.g., time of peak diurnal amplitude) categories. These statistics are then combined with analyses of high altitude aircraft observations of electrified clouds to produce the seasonal diurnal variation in the global electric circuit. Continental results display strong diurnal variation, with a lightning peak in the late afternoon and a minimum in late morning. In geographical regions dominated by large mesoscale convective systems, the peak in the diurnal curve shifts toward late evening or early morning hours. The maximum seasonal diurnal flash rate occurs in June–August, corresponding to the Northern Hemisphere summer, while the minimum occurs in December–February. Summer lightning dominates over winter activity and springtime lightning dominates over fall activity at most continental locations. Oceanic lightning exhibits minimal diurnal variation, but morning hours are slightly enhanced over afternoon. As was found earlier, for the annual diurnal variation, using basic assumptions about the mean storm currents as a function of flash rate and location (i.e., land/ocean), our seasonal estimates of the current in the global electric circuit provide an excellent match with independent measurements of the seasonal Carnegie curve diurnal variations. The maximum (minimum) total mean current of 2.4 kA (1.7 kA) is found during Northern Hemisphere summer (winter). Land thunderstorms supply about one half (52%) of the total global current. Ocean thunderstorms contribute about one third (31%) and the non-lightning producing ocean electrified shower clouds (ESCs) supply one sixth (15%) of the total global current. Land ESCs make only a small contribution (2%).

Published by Elsevier B.V.

1. Introduction

Starting with the Optical Transient Detector (OTD) in April 1995, and continuing with the Lightning Imaging Sensor (LIS) in November 1997, we have been monitoring global lightning activity with high detection efficiencies from low Earth orbit for over 17 years. We have used fifteen years of observations from these sensors (1995–2000 for OTD, 1998–2010 for LIS) to provide quantitative data on the annual and seasonal

* Corresponding author at: NASA MSFC NSSTC, 320 Sparkman Drive, Huntsville, AL 35805, USA. Tel.: +1 256 961 7962; fax: +1 256 961 7979.
E-mail addresses: rich.blakeslee@nasa.gov (R.J. Blakeslee), dmach@nasa.gov (D.M. Mach), monte.bateman@nasa.gov (M.G. Bateman), jeffrey.c.bailey@nasa.gov (J.C. Bailey).

worldwide lightning occurrences (Christian et al., 2003; Boccippio et al., 2000a,b). Our prior and current work with this ever expanding dataset has provided insights into the global spatial and temporal distribution of lightning, including the diurnal variation in flash rates (e.g., Boccippio et al., 2000b; Christian et al., 2003; Mach et al., 2011).

Also spanning a period of more than fifteen years (1993–2010), our observations from high altitude aircraft missions (e.g., Blakeslee et al., 1989; Mach et al., 2009; Hood et al., 2006) provide a varied atmospheric electrical data set, which are complementary to the satellite lightning observations. The aircraft measurements include electric fields, flash rates, and electrical conductivities. We have used the data from the overflights of electrified clouds and thunderstorms to determine storm-level atmospheric electrical parameters such as current densities, flash rates, and total current output, often called the Wilson current (Mach et al., 2009, 2010, 2011). The overflight observations and analyses have also been combined with the satellite-based data to produce results unobtainable with either dataset alone (Mach et al., 2011).

Current flowing in the global electric circuit can be calculated by combining the high altitude aircraft observations of electrified clouds (storm flash rates, electric fields, and conductivities) with the annual diurnal lightning statistics derived from OTD and LIS, and making basic assumptions about the storm current as a function of flash rate and location (i.e., land/ocean). Using this approach, Mach et al. (2011) reproduced the diurnal variations in the global electric circuit that closely matched independent measurements of the diurnal variations of the fair weather electric field obtained by the Carnegie and Maud research ships (e.g., Whipple, 1929; Torreson et al., 1946) and other subsequent measurements (e.g., Markson, 1976, 1977; Burns et al., 2005). The significance of Mach et al. (2011), and also Liu et al. (2010), which applied an alternate approach, is that these papers appear to finally confirm the long held hypothesis that thunderstorms and other electrified clouds (e.g., Wilson, 1921; Williams, 2009) are the source of the fair weather electric field variations, commonly called the Carnegie curve. These results finally overcome the long observed amplitude overestimation discrepancy that arises when using thunderday-only or lightning-only statistics (Whipple, 1929; Whipple and Scrase, 1936; Williams and Heckman, 1993; Blakeslee et al., 1999; Bailey et al., 2007).

Our present analysis has two primary objectives. First, we investigate the occurrence and distribution of lightning flashes in the annual and seasonal diurnal cycles as a function of local and universal time using reprocessed combined OTD/LIS observations to extend the prior data set (e.g., Bailey et al., 2007) by five additional years through December 2010 (now providing 15 years of OTD/LIS data in place of the previous 10 years). The results from these analyses provide new insights into the timing and distribution of lightning on a regional and seasonal basis, while continuing to confirm earlier results on mean global flash rate (Christian et al., 2003; Bailey et al., 2007). Second, we extend the work of Mach et al. (2011) by combining our reprocessed satellite-based global lightning statistics with analyses of high altitude aircraft observations of electrified clouds (Mach et al., 2009, 2010) to produce the seasonal diurnal variation in the global electric circuit. In support of this present effort, we have added storm overflight data from the Genesis and Rapid Intensification Processes (GRIP) field program (Braun et al., 2012), which has increased our storm overflight database by 25% from 850 to 1063 overflights. As in Mach et al. (2011), the seasonal diurnal variations of the global current derived from the combined satellite and airborne data analyses of thunderstorms and non-lightning producing electrified shower clouds (ESCs) closely match direct measurements of fair weather electric field variations (e.g., Torreson et al., 1946; Burns et al., 2005). This result, now shown on shorter seasonal time scales, strengthens the evidence for thunderstorms and ESCs being the source of the global electric circuit and the quantitative explanation presented in Mach et al. (2011) on how these storms contribute current into the circuit. Following the operational definition used in our prior papers (Mach et al., 2009, 2010, 2011), an ESC is defined as any storm in the dataset that had no lightning during an aircraft overpass. No other criteria, such as minimum cloud height or minimum electric field amplitude, were applied. Note that the time span of the overpass was the time when the aircraft was close enough to the storm to detect lightning. Across the various aircraft platforms, this "view time" was on the order of 1–2 min. Self consistency in this definition exists between the aircraft and low Earth orbit lightning observations used in this paper, since the satellite view time was also on the order of 1 to 2 min (e.g., Mach et al., 2009, 2010, 2011; Boccippio et al., 2002).

2. Instrumentation and measurements

2.1. Satellite observations

For global lightning statistics, we use the satellite-based total lightning dataset derived from the OTD and LIS instruments. OTD and LIS detect lightning during both day and night with a detection efficiency ranging from $44 \pm 9\%$ (OTD daytime) to greater than $93 \pm 9\%$ (LIS nighttime), storm scale location accuracy (10 km for OTD, 4 km for LIS), and small regional bias (Boccippio et al., 2002). The OTD (Christian et al., 1996) was launched in April 1995 into a 70° inclination (detects lightning to ~$\pm 75°$ latitude), 735 km altitude orbit on the MicroLab-1 satellite (later renamed OV-1). OTD collected observations for a 5-year period that ended March 2000. The LIS, launched in November 1997 on-board the Tropical Rainfall Measuring Mission (TRMM) (Kummerow et al., 1998, 2000) satellite into a 35° inclination (detects lightning to ~$\pm 38°$ latitude), 350 km altitude orbit (raised to 402 km in August 2001), remains operational (as of 2012). In this paper, we analyze LIS data from launch through 2010, which includes 5 additional years of LIS data from that used in Mach et al. (2011). Poleward of $\pm 37.5°$ latitude, only the 5 years of OTD data contribute to the combined OTD/LIS lightning climatology, which essentially is a full global climatology as there is very little lightning beyond $\pm 75°$ latitude (e.g., Orville and Henderson, 1986; Orville et al., 2011; Virts et al., submitted for publication). On an annual basis, LIS detects 90% of the lightning in the Northern Hemisphere (NH) and 98.6% in the Southern Hemisphere (SH), but this is seasonally dependent (maximum missed by LIS is 28% in NH in July, 3% in SH in January, minimum missed by LIS is 1% in both hemispheres). Several studies (e.g., Christian et al., 1996, 1999, 2003; Boccippio et al., 2000a,b; Koshak et al., 2000; Cecil et al., 2014–this issue) discuss the details of the OTD and LIS instruments and the orbital

data sets. The uncertainty of these data are on the order of 10–15%.

In this paper, 2-hour gridded flash products ($2.5° \times 2.5°$ resolution bins) are employed from the combined OTD and LIS archive, corrected for detection efficiency and view time, and appropriately averaged in time (55 days) to minimize the effects of aliasing the diurnal cycle due to the orbit precession (Boccippio et al., 2000a,b, 2002). The 2-hour binned data set assures that sufficient data are available to provide robust seasonal statistics. We initially processed the 2-hour, 365-day data file (LRADC_COM_SMFR2) from the combined OTD/LIS hierarchical data format (HDF) archive described by Cecil et al. (2014–this issue). However, it was discovered that these data had a 7.5-degree spatial smoothing that caused continental lightning to contaminate the ocean signal (and to a lesser degree, ocean data to contaminate land data). To avoid this contamination, the 2-hour data were reprocessed starting with unsmoothed data (available from the archive only by special request), corrected only for detection efficiency as a function of time. First, a 55-day temporal smoothing was applied separately to the flash counts and to the view times ($km^2 s$) at each grid point from the combined OTD/LIS file. Smoothing with a 55-day boxcar moving average removes the strong diurnal bias introduced by the orbital precession of OTD and LIS (Christian et al., 2003; Cecil et al., 2014–this issue). Next the ratio of flash counts divided by view time was calculated. Finally, the ratio at each grid point was multiplied by the grid box area to get a final result in flashes per second. The annual diurnal lightning statistics presented previously (Bailey et al., 2007; Mach et al., 2011) were derived using the 1-hour, 1-year binned data file (LRDC_COM_FR), from which it is not possible to extract seasonal results. The annual results presented in this paper are derived from the reprocessed 2-hour data set, but are in excellent agreement with the previous annual results derived from the 1-hour binned data (e.g., Fig. 1 in Mach et al., 2010).

2.2. Aircraft observations

The 1063 overflights of electrified clouds were obtained from three different aircraft flown in 11 airborne campaigns spanning 17 years from 1993 to 2010 (Table 1). Fig. 1, updated from Mach et al. (2009), shows the geographical locations of the overflight data of both land and ocean storms that span regions including the southern United States, the western Atlantic Ocean, the Gulf of Mexico, Central America, (and adjacent oceans), central Brazil, and the South Pacific. The NASA ER-2 (Heymsfield, et al., 2001; Hood et al., 2006) operates at a nominal altitude of 20 km and speed of about $210 m s^{-1}$. The General Atomics Altus aircraft (Blakeslee et al., 2002; Mach et al., 2005; Farrell et al., 2006) operates at a nominal altitude of 15 km with a speed of about $35 m s^{-1}$. Detailed information about the ER-2 and Altus aircraft systems is contained in Mach et al. (2009). The NASA Global Hawk (Ivancic and Sullivan, 2010; Ivancic et al., 2011) operates at a nominal altitude of 18 km and speed of $175 m s^{-1}$. Like the Altus, the Global Hawk aircraft is remotely piloted. NASA currently operates the Global Hawk with a maximum flight duration on the order of 26 h. All aircraft were directed to target storms based on mission objectives, remote sensing data, and pilot discretion (which in some cases meant avoiding direct overpasses of storms).

The NASA ER-2 aircraft and the Altus carried a full set of electrical instruments (electric fields and conductivity) while the Global Hawk made only electric field measurements during GRIP. The storm electric fields were measured using
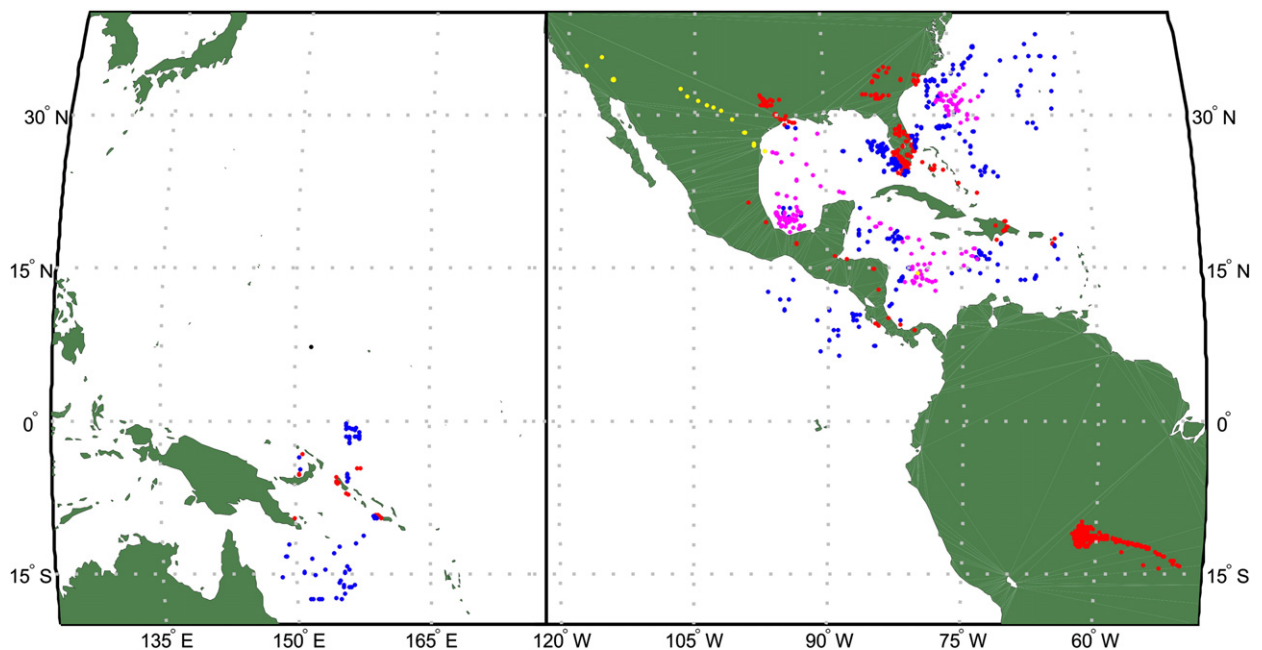

Fig. 1. Partial world map showing location of all storm overflights used in this analysis. Each dot represents a single storm overflight. The pink (yellow) dots are overflights of storms over ocean (land) from the GRIP program (Braun et al., 2012). The blue (red) dots are from storms over ocean (land) from the other field programs (Mach et al., 2010).

Table 1
Overflight data used in this analysis. This is the same dataset used in the Mach et al. (2009, 2010, 2011) analysis augmented by the addition of data from GRIP.

Campaign (month, year)	With lightning	Without lightning	Land	Oceanic	Total overflights
TOGA-COARE (Jan–Mar, 1993)	14	64	19	59	78
CAMEX-1 (Sep–Oct, 1993)	13	25	15	23	38
CAMEX-2 (Aug–Sep, 1995)	29	7	11	25	36
TEFLUN-A (Apr–May, 1998)	39	8	43	4	47
TEFLUN-B (Aug–Sep, 1998)	35	3	35	3	38
CAMEX-3 (Aug–Sep, 1998)	37	38	19	56	75
TRMM-LBA (Jan–Feb, 1999)	192	63	255	0	255
CAMEX-4 (Aug–Sep, 2001)	52	35	22	65	87
ACES (Aug, 2002)	76	22	80	18	98
TCSP (Jul, 2005)	54	44	15	83	98
GRIP (Aug–Sep, 2010)	48	165	11	202	213
Totals	589	474	525	538	1063

low noise, wide dynamic range electric field mills (Bateman et al., 2007). The conductivity observations were directly measured using Gerdien capacitor conductivity probes for the ER-2 and Altus flights. The conductivity for the GRIP overflights was estimated using nominal mean values at the Global Hawk altitude based on prior datasets (e.g., Gringel et al., 1986). We did not attempt to adjust the nominal values for small deviation associated with the solar cycle (difference in conductivity from solar minimum to solar maximum at the 35° to 40° geomagnetic latitude is about 7%) since we are confident that such a small deviation from the nominal value will not add significantly to the overall conductivity error. A detailed discussion of the instrumentation (description, calibration and errors) and the dataset processing (resultant storm currents as a function of location and flash rate, and associated errors) are given in Mach et al. (2009). The uncertainty of storm currents derived from the airborne observations is estimated to be the order of 10–15%.

Descriptions of the various field programs in which these data were collected, with the exception of the GRIP program, are contained in Mach et al. (2009). The GRIP program (Braun et al., 2012) was a NASA Earth science field experiment with Global Hawk flights in August and September of 2010 (see Table 1). Although there were only five missions flown, the long flight durations of the Global Hawk (up to 26 h), augmented our prior aircraft overflight data by 25%, increasing our overflight database from 850 (Mach et al., 2009) to 1063 storm overpasses.

3. Analysis and results

3.1. Annual and seasonal diurnal lightning variation

For our analysis of the global lightning activity, the land and ocean contributions were isolated by applying the

"continental" mask shown in Fig. 2 to the combined OTD/LIS gridded data. In addition, the continental mask was further subdivided in order to identify the specific contributions to the global lightning from the different continental regions and the ocean. The regions, in descending order of their annual flash rate, include Africa, South America, Asia, the oceans, North America, Australia/ Maritime Continent, and Europe.

Fig. 3, derived from the combined OTD/LIS data set, shows the global annual diurnal lightning variation for the entire world, the continental regions, and the oceans in both universal (UTC, upper plot) and local (LT, lower plot) time. All continents display a strong diurnal variation, with the lightning activity peaking in the late afternoon between 1500 and 1700 LT, while a minimum of activity occurs in the late morning hours between 0900 and 1100 LT. The diurnal amplitudes are different for different continents, with the highest amplitude over Africa and the lowest over Europe. Oceanic lightning exhibits only minimal (i.e., nearly flat) diurnal variation, but morning hours are typically slightly enhanced over afternoon. The geographical distribution of peak diurnal lightning activity (local time) for land and ocean is illustrated in Fig. 4. In regions of the world dominated by large mesoscale convective systems such as the Central US, Argentina, and West Africa, the peak in the diurnal curve shifts toward late evening or early morning hours (Wallace, 1975; Zipser et al., 2006; Ogawa and Komatsu, 2009). Consistent with the integrated result captured in Fig. 3, the local time of peak diurnal activity in the oceans tends toward late evening through early morning. The variance over the oceans is typically higher than over land due to the smaller quantity of lightning data per grid box and the flatter diurnal behavior. This is reflected in Fig. 4 by the scatter in peak times often found in adjacent pixels.

We compare the seasonal diurnal flash rates for the world in UTC and LT in Fig. 5. The maximum seasonal diurnal flash rate occurs in June–August (JJA) corresponding to the NH summer, when greatly enhanced lightning activity from the North American and Asian continents combine with the large, steady contribution (across all seasons) from Africa. The September-November (SON) period exceeds March-May (MAM), due to the much enhanced South American contribution that occurs during SON. The minimum seasonal diurnal flash rate occurs in December-February (DJF) during the SH summer tracing to the overall much smaller land mass present in the SH, and the proportionate decease in lightning activity as a result.

A four panel view in UTC highlighting details of how and when the different global regions contribute to each of the seasonal diurnal curves is given in Fig. 6. Throughout all seasons, Africa provides the largest single contribution to the diurnal cycle. Also, throughout the seasons of the year, the lightning contribution from oceanic regions remains relatively constant and exhibits a flat diurnal response. During JJA in NH summer (lower left panel), enhanced activity in North America and Asia joins that of Africa to contribute equally to the total global flash rate. Europe also provides its greatest input at this time, and although greatly diminished from other seasons, South America still provides a contribution exceeding that of Europe. Moving into SON during the SH spring (lower right panel), South America provides
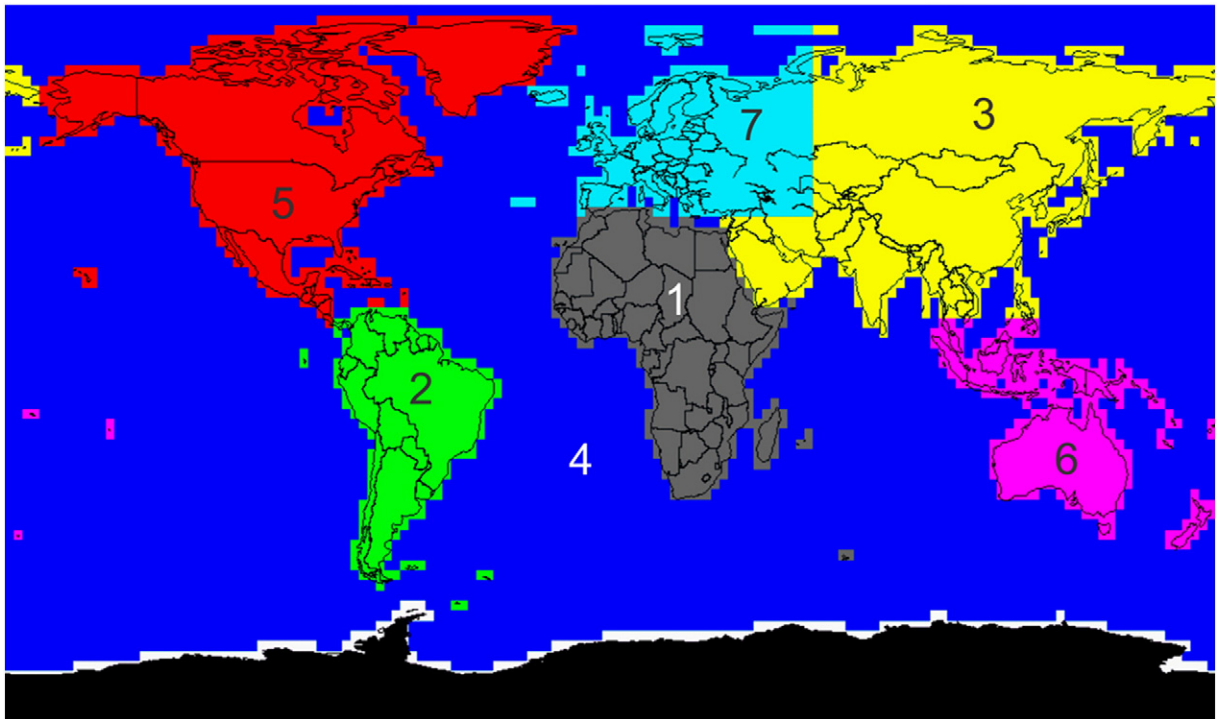
Fig. 2. Continental (and ocean) mask used for this study. The regions are ordered based on their annual flash rate (see Table 2). Africa is region 1 (grey, black in subsequent line plots), South America is region 2 (green), Asia is region 3 (yellow), oceans are region 4 (blue), North America is region 5 (red), Australia/ Maritime Continent are region 6 (magenta), and Europe is region 7 (cyan).
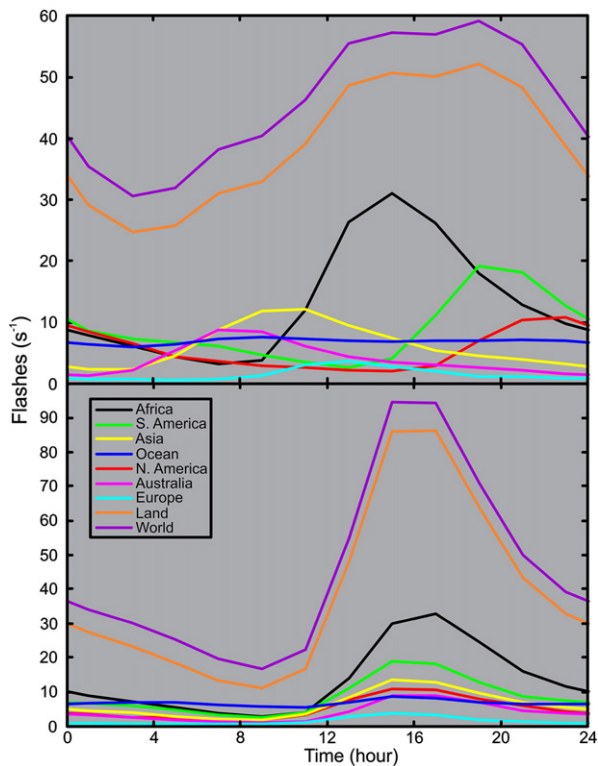

Fig. 3. Annual diurnal flash rate derived from the combined OTD/LIS data in UTC (top plot) and local time (bottom plot).

an enhanced contribution approaching that of Africa and Australia/Maritime Continent begins to ramp up its activity, while contributions from North America and Asia decline significantly. South American lightning contributions remain prominent during DJF in SH summer (upper left panel), although at a slightly lower rate than in SON, while the Australia/Maritime Continent lightning rate increases by 50% at this time. Finally, during MAM (upper right panel), South America declines by more than half. Also, the lightning contribution from Asia becomes comparable to that of South America, while North American activity begins to increase.

Table 2 summarizes the annual and seasonal mean flash rates for the world and other regions. The mean lightning activity of the continents located in either the northern or southern hemisphere follows in descending amplitude a seasonal order of summer, spring, fall, and winter. Noteworthy results are in blue italicized text. In South America which mostly lies in the SH, spring activity (SON) slightly exceeds the summer (DJF) activity. Africa, which straddles the equator, exhibits a small semi-annual signal in the flash rate (manifested by a slight enhancement during the MAM and SON seasons), but as previously noted, the African activity is comparable in every season. For the world, the maximum mean flash rate (55.7 flashes/s) occurs during JJA (NH summer) and the minimum (35.9 flashes/s) occurs in DJF (NH winter). The mean global flash rate for the other seasons (MAM, SON) falls in between these values (47.2 flashes/s in SON and 44.1 flashes/s in MAM).
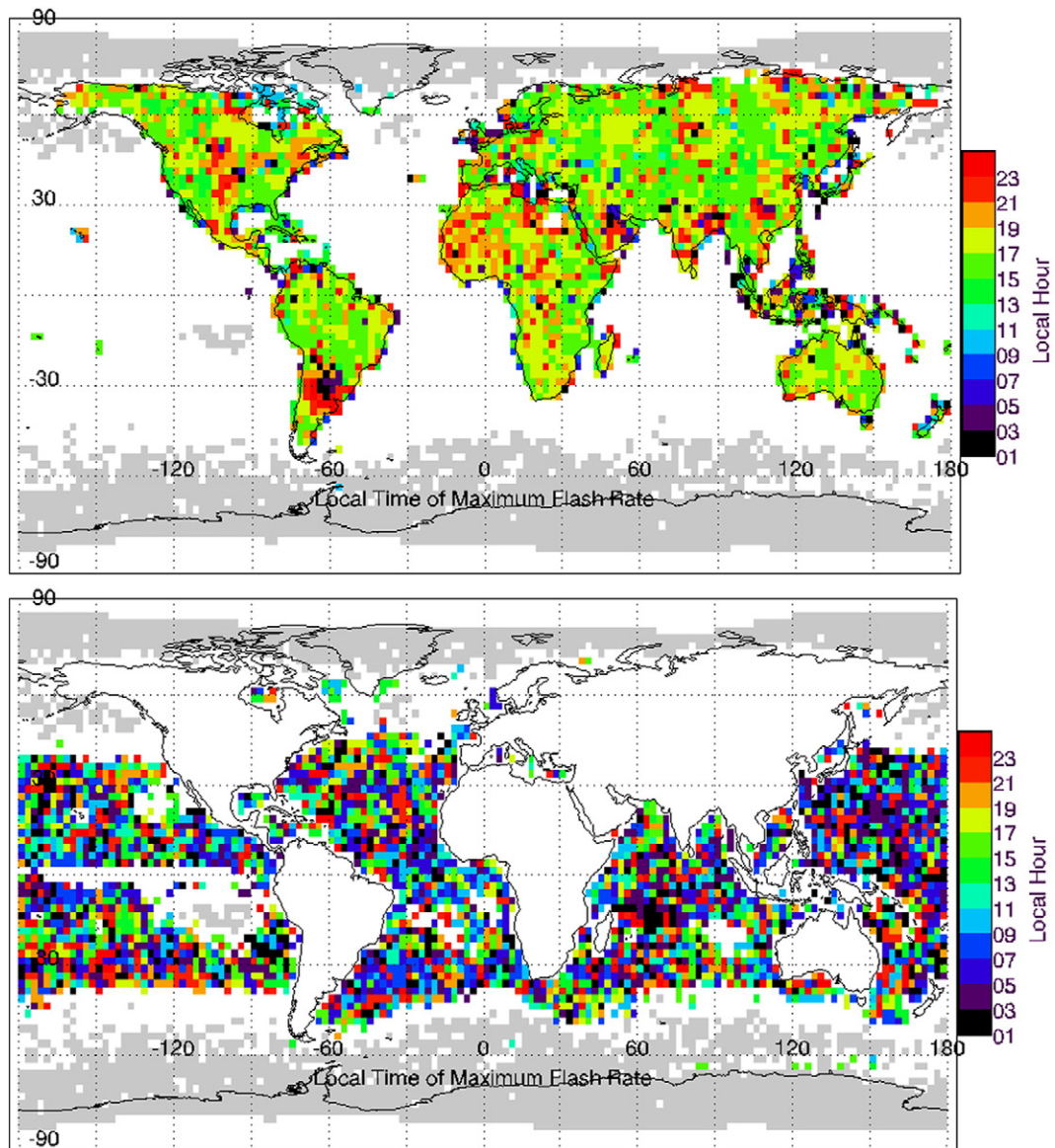
Fig. 4. Local time of peak lightning rates for land (upper panel) and ocean (lower panel). Grey areas represent grid points with no lightning counts registered. The OTD field-of-view did not extend beyond the northern or southern edge of the grey area. White areas within the combined satellite viewing range represent grid points with fewer than 50 flashes.

3.2. Seasonal diurnal current determination

By combining the seasonal diurnal lightning rates from Fig. 6 with the overflight data from Mach et al. (2009, 2010, 2011), enhanced with GRIP data, we can estimate the seasonal variation in the global electric circuit. The overflight storms are summarized by category (land/ocean and lightning/non-lightning) in Tables 1 and 3. They are the same data used in Mach et al. (2009, 2010, 2011) with the addition of data from the GRIP flights (Braun et al., 2012). With two exceptions, we used the same analysis method to process the overflights from GRIP as were applied in Mach et al. (2009). The first exception is that there were no on-board conductivity measurements for the GRIP overflights. However, as discussed in Section 2.2, we

do not believe that the use of these data significantly increased the conductivity error bounds. The second exception is that many overflights in the GRIP program were not well centered on the storms of interest. This exception means that few additional Wilson currents are added to our storm current statistics from the GRIP dataset as the "near miss" assumptions used in the prior analysis (i.e., Mach et al., 2009) are not valid. However, the GRIP overpasses were still close enough to measure storm polarity, lightning rates, and storm locations.

The first step toward calculating seasonal variation in the global electric circuit from airborne and satellite observations is to derive land and ocean seasonal diurnal flash rates from the OTD/LIS dataset. This result is presented in Section 3.1 (Fig. 6). The pertinent total land and ocean diurnal flash rate curves are
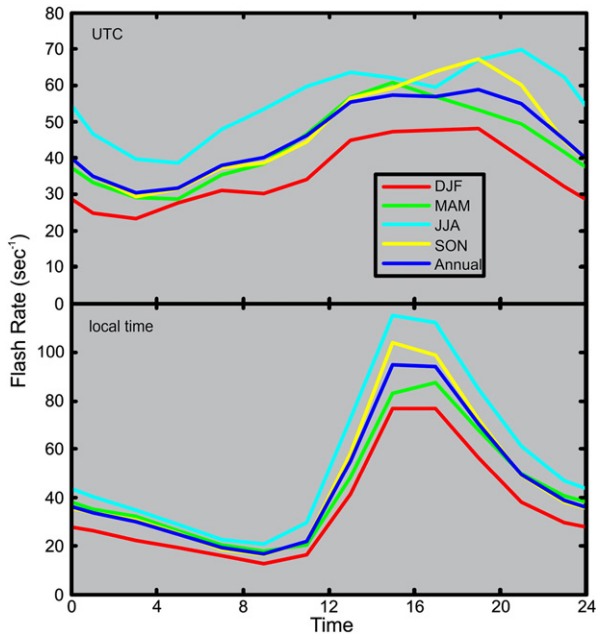
Fig. 5. Seasonal diurnal flash rates in UTC (top plot) and LT (bottom plot) derived from the combined OTD/LIS data.

reproduced in Fig. 7. The next step is to convert the flash rates in Fig. 7 into storm counts based on the mean flash rate per storm derived from the overflight dataset for land and ocean storms. We adopted the same definition of a "land" and "ocean" storm in the overflight dataset as used in Mach et al. (2010; 2011), namely that any storm within 25 km of a landmass, based on

the National Geophysical Data Center gridded digital elevation model (ETOPO2v2) (U.S. Department of Commerce, 2007), is considered a land storm while any storm exceeding this range is considered an ocean storm. Mach et al. (2010) found a significant difference between the mean storm flash rate of land (1.7 flashes min^{-1}) and ocean (0.33 flashes min^{-1}) storms. With the addition of the GRIP data, the mean flash rate for land storms remained 1.7 flashes min^{-1} while the ocean storm flash rate declined slightly to 0.28 flashes min^{-1}. Dividing the satellite-derived diurnal flash rates (Fig. 7) by the airborne-derived mean flash rate per storm yields the diurnal variation in land and ocean storm counts (Fig. 8). The resulting storm counts include both thunderstorms and storms with no lightning (i.e., ESCs), because the airborne-derived mean storm flash rates include all electrified storms.

Next, we multiply the total storm counts in Fig. 8 by the fraction of storms with and without lightning listed in Table 3 to generate Fig. 9—the number of storms over land and over ocean with and without lightning (i.e., thunderstorms and ESCs). Table 3 includes the overflight dataset used in Mach et al. (2010; 2011), adjusted by the GRIP data. The majority of land storms have lightning (77%) while the majority of ocean storms do not (66%).

As the final step in the analysis process, we take the storm counts in Fig. 9 and multiply them by the mean storm currents (i.e., over land and over ocean, with lightning and without lightning) given in Table 4 (Mach et al., 2010, 2011) to derive the seasonal changes in the diurnal variation of the global electric circuit (Fig. 10). The maximum total mean current occurs in the NH summer (2.4 kA) while the minimum total mean current is found in the NH winter (1.7 kA). The total mean current values during NH spring
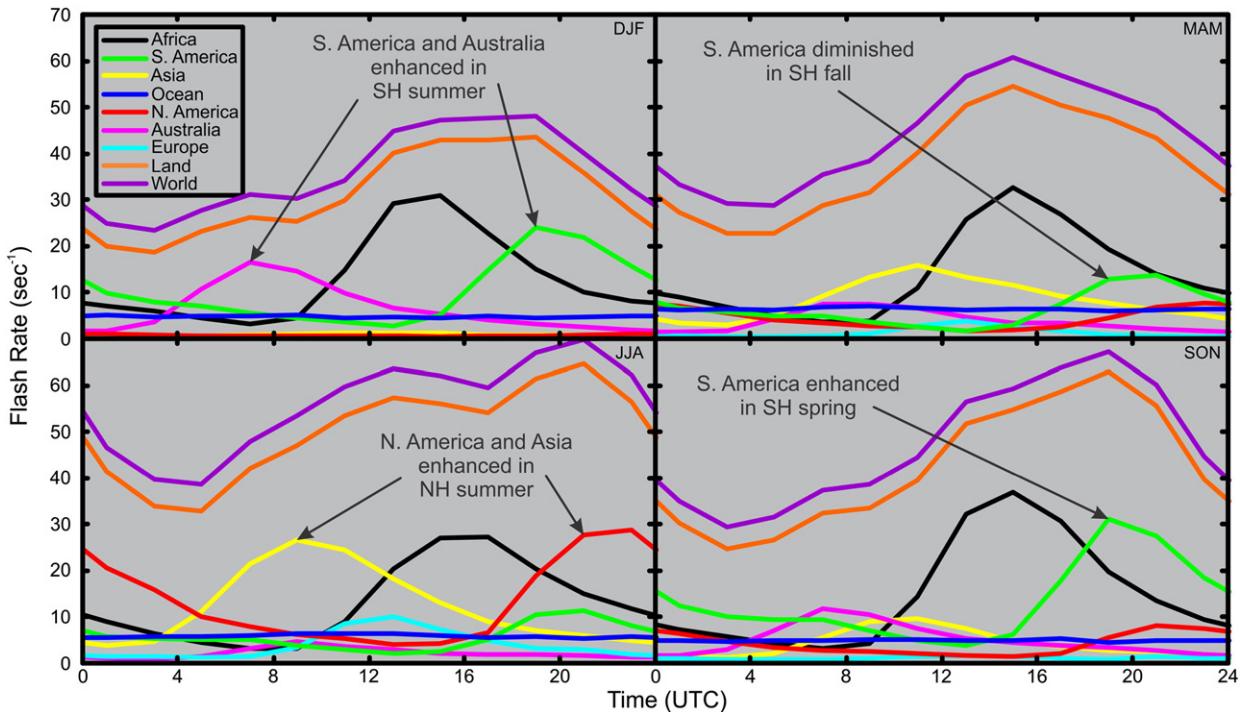

Fig. 6. The panels depict the seasonal diurnal flash rate variation (UTC) for total world, the land and ocean regions, and the individual continents identified in Fig. 2 for DJF (top left), JJA (bottom left), MAM (top right), and SON (bottom right).

Table 2

Annual and seasonal lightning flash rates (flashes/s) for world, world<37.5° (i.e., LIS orbital extent), land, oceans, and continents (deviations from usual season order noted by blue italicized entries and discussed in the text).

Region	Annual	Annual %	DJF	DJF %	MAM	MAM %	JJA	JJA %	SON	SON %	Season Order	Local Season Order
World	45.7	100.0	35.9	100.0	44.1	100.0	55.7	100.0	47.2	100.0	JJA,SON,MAM,DJF	N/A
World<37.5°	40.7	89.1	34.9	97.2	40.9	92.8	42.5	76.2	44.6	94.5	*SON,JJA,MAM,DJF*	N/A
Land	40.3	88.2	31.2	87.0	37.7	85.6	49.9	89.6	42.2	89.4	JJA,SON,MAM,DJF	N/A
Ocean	5.4	11.8	4.7	13.0	6.3	14.4	5.8	10.4	4.8	10.2	MAM,JJA,SON,DJF	N/A
Africa	13.7	30.0	12.9	36.0	13.9	31.6	13.0	23.3	15.0	31.7	*SON,MAM,JJA,DJF*	N/A
S. America	8.8	19.1	10.1	28.1	6.3	14.3	5.6	10.0	13.1	27.7	*SON,DJF,MAM,JJA*	*Spring,Summer,Fall,Winter*
Asia	6.5	14.2	0.8	2.4	8.4	19.0	12.4	22.3	4.2	8.9	JJA,MAM,SON,DJF	Summer,Spring,Fall,Winter
Ocean	5.4	11.8	4.7	13.0	6.3	14.4	5.8	10.4	4.8	10.2	MAM,JJA,SON,DJF	N/A
N. America	5.4	11.8	0.6	1.7	4.1	9.3	12.9	23.2	3.9	8.3	JJA,MAM,SON,DJF	Summer,Spring,Fall,Winter
Aust	4.4	9.7	6.5	18.2	3.8	8.7	2.2	3.9	5.1	10.9	DJF,SON,MAM,JJA	Summer,Spring,Fall,Winter
Europe	1.6	3.5	0.2	0.5	1.2	2.7	3.9	6.9	1.1	2.3	JJA,MAM,SON,DJF	Summer,Spring,Fall,Winter

(MAM) and fall (SON) are between the NH summer and winter values (2.2 kA and 2.1 kA, respectively). Detailed statistics, including the mean values and percentage contribution of the seasonal and annual components of the global electric circuit are summarized in Table 5.

4. Discussion

4.1. Seasonal variation in the total global lightning statistics

Analyses of seasonal lightning distribution maps yield additional insights pertinent to a better understanding of the diurnal variation. Fig. 11 shows the seasonal distribution of mean flash rate over the world. Difference maps (Fig. 12), derived by taking the difference between distribution maps of opposite seasons (i.e., JJA–DJF, DJF–JJA, MAM–SON, and SON–MAM) and plotting only positive values, show in which season (summer versus winter, spring versus fall) a location on the Earth has greater lightning occurrence. Not unexpectedly over land, summer lightning dominates winter activity, with lightning in Northern Hemisphere summer (JJA) greatly exceeding that found in Southern Hemisphere summer (DJF), due to its much greater land mass. This is also reflected in the results presented previously in Figs. 5 and 6. The difference analysis also reveals that springtime lightning dominates fall lightning at most locations; however, there are several exceptions to this behavior including central Canada and the west coast of California and Mexico. The springtime lightning signal is strongly manifested over the Amazon region in South America. There may be many reasons for this behavior. Often more electrically active storms occur at the onset of the rainy season. Also, many authors have attributed increased storm intensity to aerosol effects associated with an extensive regional burning season. The diminishing lightning activity in the South America fall (MAM) may even partially be a manifestation of the "green ocean" effect (Williams et al., 2002).

Table 3

Counts (fractions) of storms with/without lightning and land/ocean based on our overflight dataset (including data from GRIP).

	Land	Ocean	Total
With lightning	406 (0.77)	183 (0.34)	589
Without lightning	119 (0.23)	355 (0.66)	474
Total	525 (1.00)	538 (1.00)	1063

In fact, similar behavior occurs, albeit to lesser degree, at many land-based locations around the Earth. In contrast to the land, the difference analyses show that over oceanic regions, lightning activity in the winter and fall months tends to exceed that in summer and spring, respectively. This result may reflect the high heat capacity of water, leading to greater convective instability over the oceans in wintertime as cold air from the continents moves over relatively warmer ocean basins. Exceptions include the vigorous convection that occurs over warm ocean currents such as the Gulf Stream off North America.

4.2. Changes in storm statistics from updated overflight data

The addition of GRIP data to the storm overflight database resulted in several small but interesting changes in the overall storm overflight statistics. The GRIP data were predominantly (95%) from ocean storms due to Global Hawk flight restrictions. The overflights were also mostly over ESCs (77%). This is in contrast to the rest of the overflights that were dominated by storms with lightning (64%). In our prior work on this topic, we speculated that the overflight database might be biased toward storms with lightning due to the target selection strategy (Mach et al., 2011). During GRIP flights, the target selection was much more random, due to the flight operations of the Global Hawk (i.e., the aircraft flight path was not modified to target more active storms with the exception of hurricane eyewall overflights). This more random target selection may have resulted in a less biased storm dataset.

The higher percentage of ESCs in the GRIP dataset also lowered the mean flash rate for all storms over the ocean from 0.33 to 0.28 flashes min^{-1}. Although the ocean storms in GRIP had a lower overall flash rate (0.20 flashes min^{-1}), the GRIP ocean storms with lightning actually had a higher flash rate (0.98 flashes min^{-1}) than the ocean storms with lightning in the previously acquired overflight database (0.77 flashes min^{-1}). Only 11 overpasses of land storms were acquired during GRIP due to severe restrictions imposed for over-land flights (these land storm overpasses all occurred during the transit flights from Edwards AFB, California to the Gulf of Mexico within an approved narrow flight corridor along the U.S.–Mexico border). The 11 land storms were still dominated by storms with lightning (64%) despite the random nature of the target selection process in GRIP for land storms (the flight path to and from the Gulf was preset). The flash rates for all land storms in GRIP were
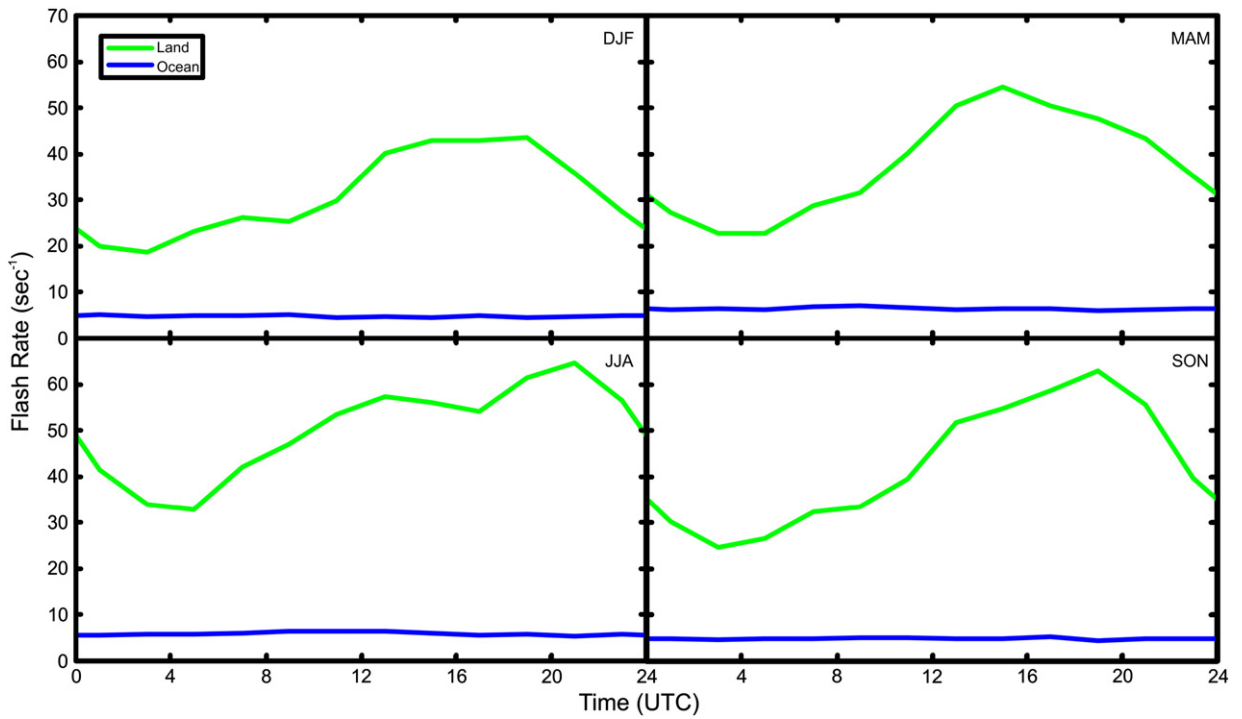
Fig. 7. Seasonal diurnal flash rate variation in UTC for land (green) and ocean (blue) extracted from Fig. 6. The total land and ocean curves are the starting point in calculating global currents from global lightning statistics. The seasons again include DJF (top left), JJA (bottom left), MAM (top right), and SON (bottom right).
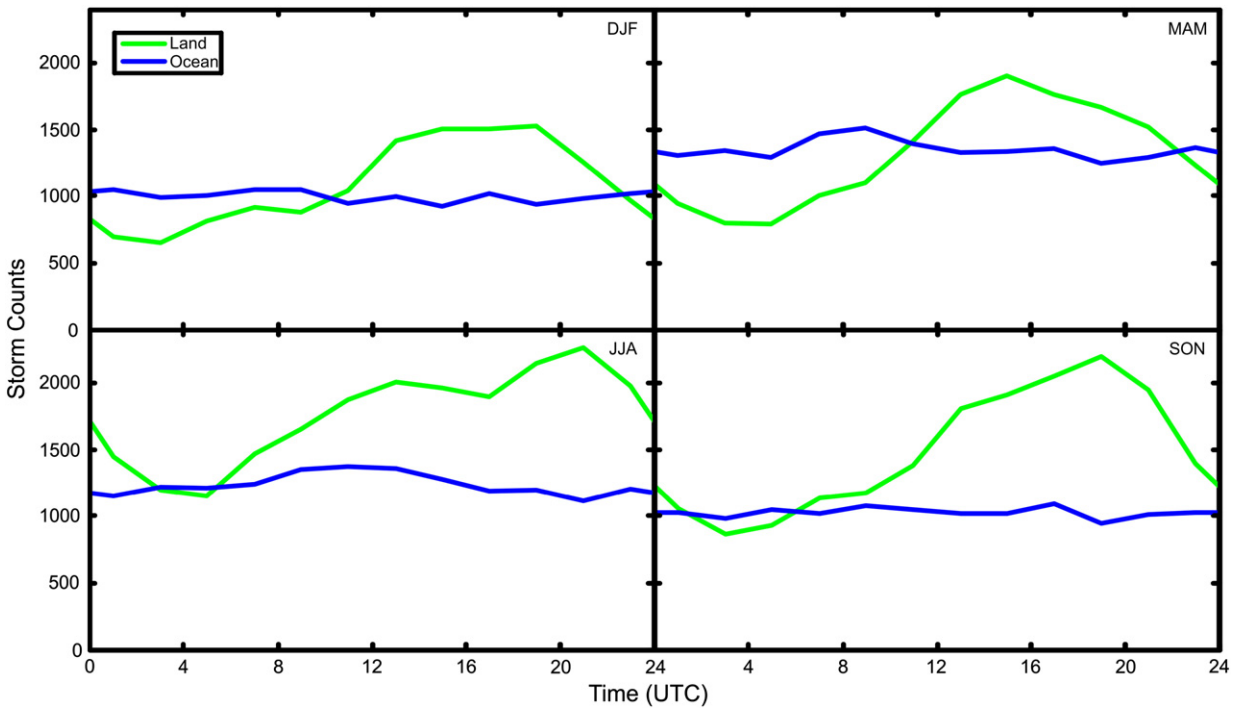

Fig. 8. The diurnal variations in storm counts for land (green) and ocean (blue) for DJF (top left), JJA (bottom left), MAM (top right), and SON (bottom right). The storm counts include both thunderstorms (electrified storms with lightning) and ESCs (electrified storm clouds without lightning).
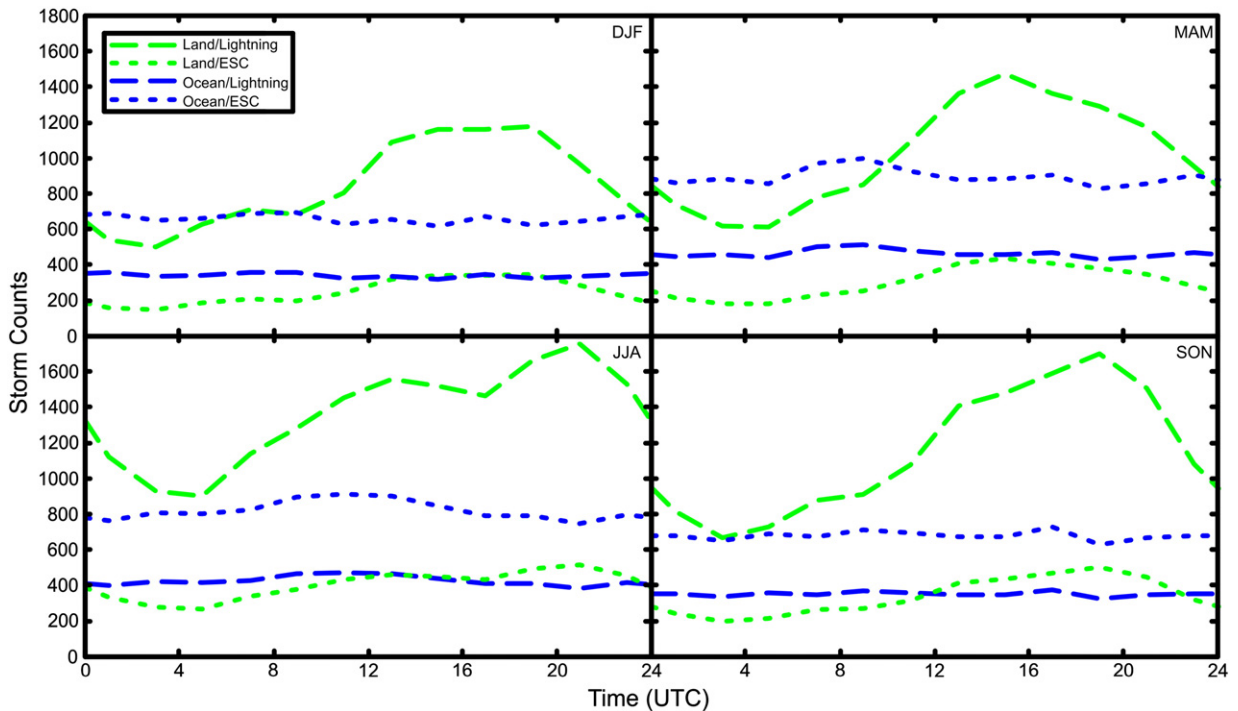
Fig. 9. The diurnal storm counts displayed for land (green) and ocean (blue) in lightning (dashed line) and non-lightning ESC (dotted line) storm categories for DJF (top left), JJA (bottom left), MAM (top right), and SON (bottom right).

larger (3.2 flashes min^{-1}) than in the prior storm overflight dataset, but due to the small fractional increase (i.e., only 2%) in the overall number of land storms, the extra GRIP land storm data did not change the mean flash rate of 1.7 flashes min^{-1} for land storms from that presented in Mach et al. (2009, 2010).

4.3. Seasonal variation in the total global current

The variations in annual and seasonal mean currents for land, ocean, and total (i.e., land plus ocean) storms are summarized in Table 5 and plotted in Fig. 13. Note that the total ocean contribution (thunderstorms plus ESCs) is comparable to the total land contribution (thunderstorms plus ESCs), and the total ocean contribution is actually greater than the land for one season (MAM). Also as was noted in Mach et al. (2011) for the annual total mean current, the seasonal total mean currents (Table 5, Figure 13) are slightly above the estimates of others (e.g., Roble and Tzur, 1986). Our estimates of the storm currents are based on measurements close to the tops of storms. Perhaps, as Mach et al. (2011) suggested earlier, some of the current present at 15–20 km may not make it to the ionosphere and contribute to the global electric circuit generator.

Table 4
Mean current (A) for storms with/without lightning and over land/ocean based on our overflight dataset.

	Land	Ocean
With lightning	1.0	1.7
Without lightning	0.13	0.41

In Mach et al. (2011), we pointed out that land storms with lightning dominate the total Wilson current on an annual basis. This remains true for each seasonal period as well. However, the storm current analyses here (Table 5 and Fig. 13) and the earlier results presented in Mach et al. (2011) indicate that when the total current inputs from lightning and ESC storms are taken into account, land and ocean storms contribute nearly equal amounts of current to the global electric circuit. We find that the total contribution of land (ocean) storms to the global electric circuit is 54% (46%). Land storms with lightning are still the single dominant component, contributing about half the total current. Ocean thunderstorms provide about one-third of the total current, which when coupled with the one-sixth contribution from ocean ESCs, tend to "even the score" between ocean and land contributions to the global electric circuit. Land ESCs provide a constant, but minuscule percentage contribution (about 2%) to the global circuit.

Whipple and Scrase (1936) postulated that ocean storms, missing in the thunderday statistics, might contribute to the global electric circuit to reduce the amplitude discrepancy that existed between the diurnal variations of thunderday (and later global lightning) statistics and global potential electric field observations. Wilson (1921) postulated that storms without lightning (ESCs) might help "flatten" the larger amplitude variation suggested by the land-based thunderstorm activity. Our results indicate that both postulations are supported at some level. However, a number of factors not postulated in the early studies are essential to quantitatively explain how storms contribute to the global electric circuit. These factors, identified in
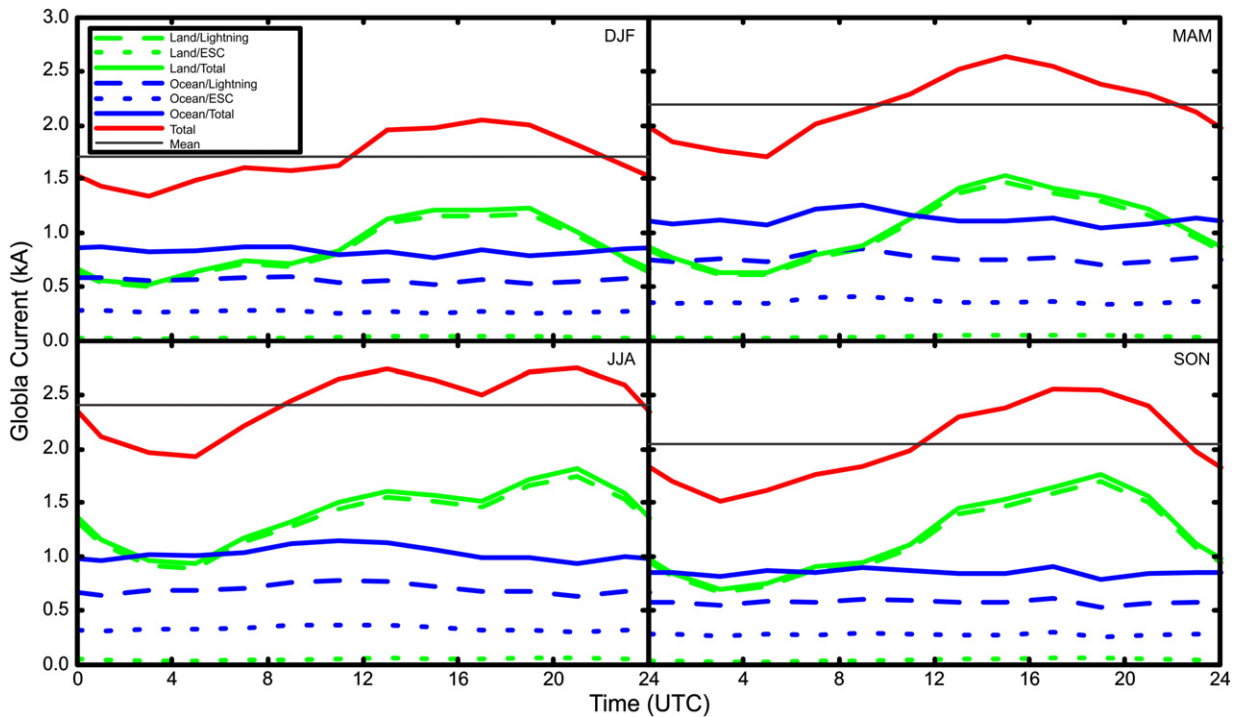
Fig. 10. Panels depict the seasonal variations of diurnal global electric circuit current due to land/ocean and lightning/non-lightning producing ESC storms. The solid lines are the summed contributions of lightning storms and ESCs. The red curve is the diurnal current from the entire Earth, while the blue and green curves are current contribution from ocean and land storms, respectively. The dotted lines are for ESCs (electrified storms without lightning), and the dashed lines are for storms with lightning. The thin black line in each panel is the global mean current for that season.

this analysis and in Mach et al. (2011), include (1) the significant land-ocean storm current output differences, (2) the flat diurnal behavior of the ocean storm activity, and (3) the significant contribution to the global circuit by ocean ESCs. Land ESCs, with their small mean current contribution of only 0.13 A per storm, contribute very little toward sustaining the global electric circuit. It appears that most land storms that become significantly electrified also produce lightning.

4.4. Comparison of seasonal global electric circuit current to other measures of the global electric circuit

Fig. 14 compares our seasonal diurnal estimates of the global electric circuit with two other independent seasonal measures of the global electric circuit. We have normalized each of the three seasonal measures of the diurnal variation of the global electric circuit to its respective mean value so

that they can be compared on an equal scale. The first is from Burns et al. (2005) and is based on monthly mean diurnal electric field observations collected at Vostok, Antarctica. We averaged the monthly means presented in Burns et al. (2005) into seasonal curves, shifted one month from the previous plots in this paper (i.e., November/December/January versus DJF, etc.) in order to match the second independent dataset. The second dataset is from Torreson et al. (1946), and corresponds to the seasonal variation in the diurnal potential gradient obtained during the Carnegie voyages. Since the Torreson et al. (1946) seasonal data are offset by one month from our analyses, we have chosen in this section to shift our seasonal estimate of the diurnal current one month (i.e., NDJ, FMA, MJJ, ASO). Given the independent measurements and the widely different methods, locations, time periods and time scales used to obtain the various curves, there is remarkable agreement among these three measures of the seasonal global electric circuit. The three normalized

Table 5
Mean current (kA) for land/ocean, lightning/ESC, and totals.

|		Annual kA (%)		DJF kA (%)		MAM kA (%)		JJA kA (%)		SON kA (%)	
Land	ESC	1.13 (54)	0.04 (2)	0.88 (51)	0.03 (2)	1.06 (48)	0.04 (2)	1.40 (58)	0.05 (2)	1.19 (58)	0.04 (2)
	Lightning		1.09 (52)		0.85 (50)		1.02 (47)		1.35 (56)		1.15 (56)
Ocean	ESC	0.96 (46)	0.31 (15)	0.83 (49)	0.27 (16)	1.13 (52)	0.37 (17)	1.03 (42)	0.33 (14)	0.86 (42)	0.28 (14)
	Lightning		0.65 (31)		0.56 (33)		0.76 (35)		0.70 (29)		0.58 (28)
Total	ESC	2.09 (100)	0.35 (17)	1.71 (100)	0.30 (18)	2.19 (100)	0.41 (19)	2.43 (100)	0.38 (16)	2.05 (100)	0.32 (16)
	Lightning		1.74 (83)		1.41 (82)		1.78 (81)		2.05 (84)		1.73 (84)
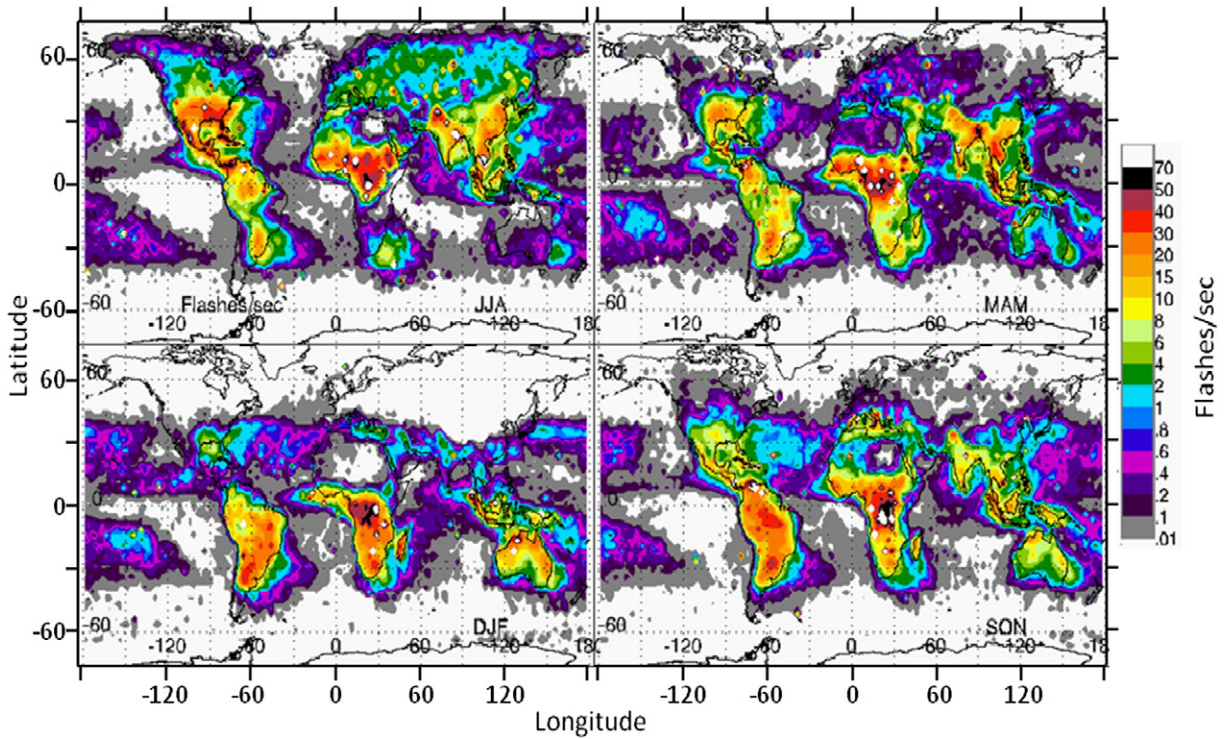
Fig. 11. Seasonal lightning distributions are shown for JJA (top left), DJF (bottom left), MAM (top right), and SON (bottom right).
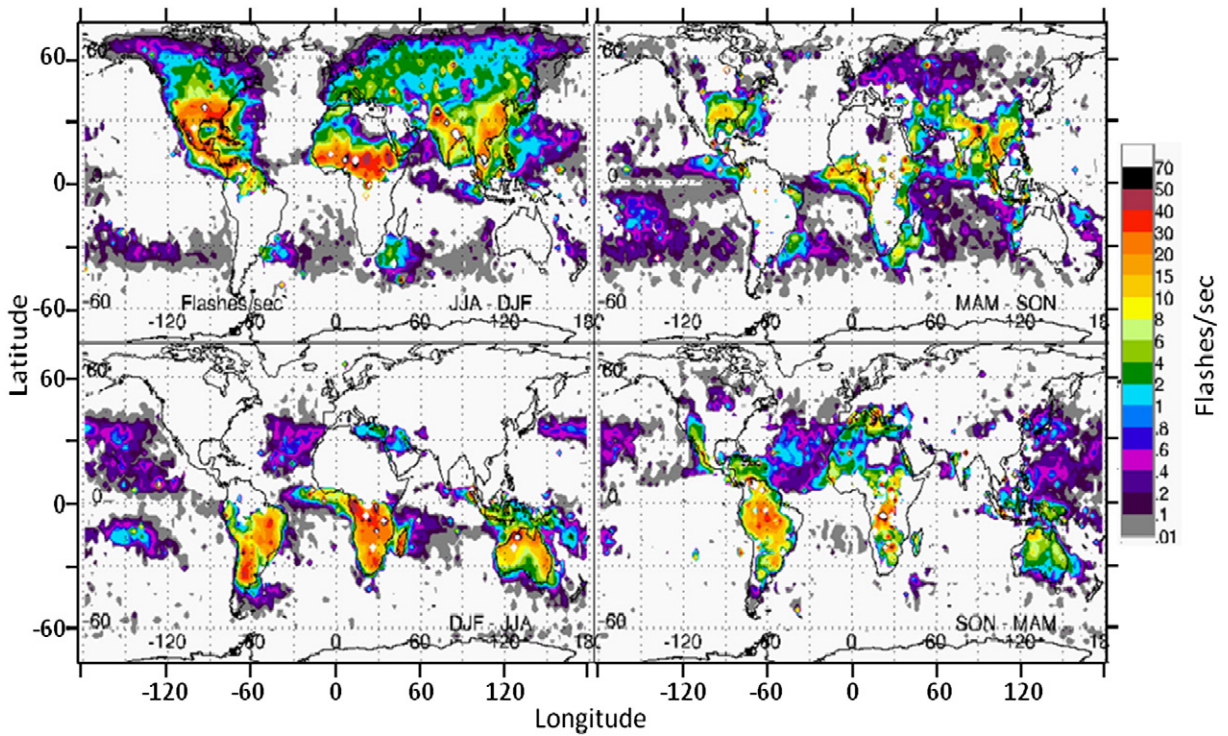

Fig. 12. Difference maps generated by taking the difference of the seasonal lightning distributions, JJA–DJF (top left), DJF–JJA (bottom left), MAM–SON (top right) and SON–MAM (bottom right), and plotting only the positive results. Over land, summer lightning dominates over winter activity (left plots) and spring lightning dominates over fall activity (right plots). Over ocean regions the opposite result typically occurs.
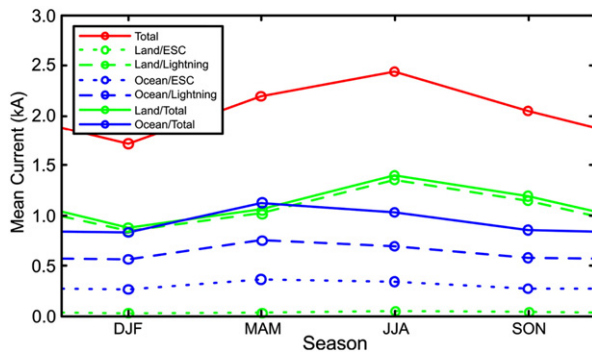
Fig. 13. Seasonal mean currents for land (green), ocean (blue), and total (red). The dotted lines (green/blue) are for ESCs, the dashed lines are for storms with lightning, and the solid lines (green/blue/red) are for all storms (lightning plus ESCs).

representations of the global electric circuit display differences that are within 15% (and often within 10%) of each other at all times, except for two short periods (one during FMA and one during MJJ). The root-mean-squared (RMS) differences among the three sets of seasonal curves are presented in Table 6. The RMS differences range from as low as 3% (Carnegie—Vostok in MJJ) to as high as 12% (Carnegie—our results in FMA). The overall differences between the Carnegie and Vostok curves are similar to those found between our result and these two analyses (and a similar result was also found when we compared our result to Vostok in the DFJ seasonal system).

Returning to Fig. 14, we observe close agreement between our current calculation and the Carnegie analyses during NDJ. The Vostok shows its widest departure during this season exceeding the other curves by about 15% at 0600 and 1900 UTC, the latter time corresponding to the strong peak in South American thunderstorm activity. During MJJ, the Vostok and Carnegie curves are in closer agreement, with our results exceeding the other two between 0800 and 1600 UTC, with the peak difference at 1300 UTC. The peak at 1300 UTC during MJJ corresponds to the joint Asian-African thunderstorm activity (i.e., similar to that shown in JJA in Fig. 6). During FMA all three curves diverge from each other between 0800 and 1700 UTC. The largest single difference of about 23% occurs in this season between our current estimate and Carnegie at 1300 UTC. Finally, during ASO, our estimate and Carnegie are again in close agreement until about 1800, when the Vostok and our data agree until 0000 UTC.

Speculations as to the sources and phases of differences among the three measures of the global electric circuit presented here are difficult because even the "major" disagreements are only on the order of 15%. None of the datasets have error bars of less than 10% (Markson, personal communication, 2010), especially on this shorter seasonal time scale. Hence, when the error limits (i.e., on the order of 10–15%) of the three datasets are considered, these three measures of the global electric circuit are essentially the same. The differences seen may simply be due to errors or different sampling techniques between the individual datasets. In addition, differences may trace to natural variability in the global electric circuit over the various time periods of the different measurements. Also, none

of the data displayed in these curves were sampled in the same years, and the sampling periods varied considerably, with our lightning-airborne dataset actually having the longest sampling duration—all of which can contribute to the variance displayed by these independent measures of the global electric circuit.

In our analyses of seasonal diurnal current, we only used a single ratio of lightning versus non-lightning for the land and another ratio for ocean but did not consider any possible seasonal variations in these ratios. There are simply not enough data to subdivide the aircraft data into seasons, as there are for dividing the data into land and ocean categories. Also, in Mach et al. (2011), we did quantitatively consider the potential bias introduced by undersampling ESCs, even though our annual diurnal current estimate already agreed with the annual Carnegie curve within the error bounds. A sensitivity analysis presented in that paper suggested that we may have undersampled ESCs by as much as a half or third (oceanic ESCs being the most significant), but the key conclusions remained essentially unaltered by the additional ESCs. Since a similar situation exists here—i.e., our seasonal diurnal current results are already in agreement within the error bounds of the Vostok and Carnegie observations—we chose not to repeat this sensitivity analysis for the seasonal case.

5. Conclusions

5.1. Seasonal variations in lightning rates

The 15-year combined OTD/LIS data are sufficient to provide good annual and seasonal diurnal flash rate characterizations. The maximum diurnal flash rate occurs during the Northern Hemisphere summer (JJA), while the minimum occurs during DJF. The specific shape and amplitude of the observed diurnal flash rate curves in universal time (UTC) for annual and seasonal periods directly reflects the integrated contributions from the various geographical regions in proportion to the lightning production within those regions as described by Whipple (1929) and Whipple and Scrase (1936). The integrated lightning activity associated with each continent in local time displays a similar strong diurnal variation, with the lightning activity peaking between 1500 and 1700 LT. However, our analysis shows that at specific locations within each continent dominated by large mesoscale convective systems, the local time of peak diurnal activity shifts toward late evening or early morning hours.

Ocean regions contribute 10–14% to the total global lightning, depending on the season. Over the oceans, although the activity tends to be slightly more enhanced in the late evening and morning hours, the overall diurnal behavior of the ocean lightning is essentially flat. However, this minimal (flat) diurnal behavior is a key factor (along with land/ocean differences in the mean currents) in resolving the long standing amplitude discrepancy that exists between the lightning-only statistics and the long standing, strongly supported Carnegie curve.

Another result from our analysis shows that summer lightning dominates over winter activity and springtime lightning dominates over fall activity at most continental locations. The analysis also shows that this behavior is reversed over many oceanic locations. As discussed in Section 4.1, there are good hypotheses to explain the dominance of summer lightning over wintertime activity over land and the reverse behavior over ocean. It is much harder to fully understand why
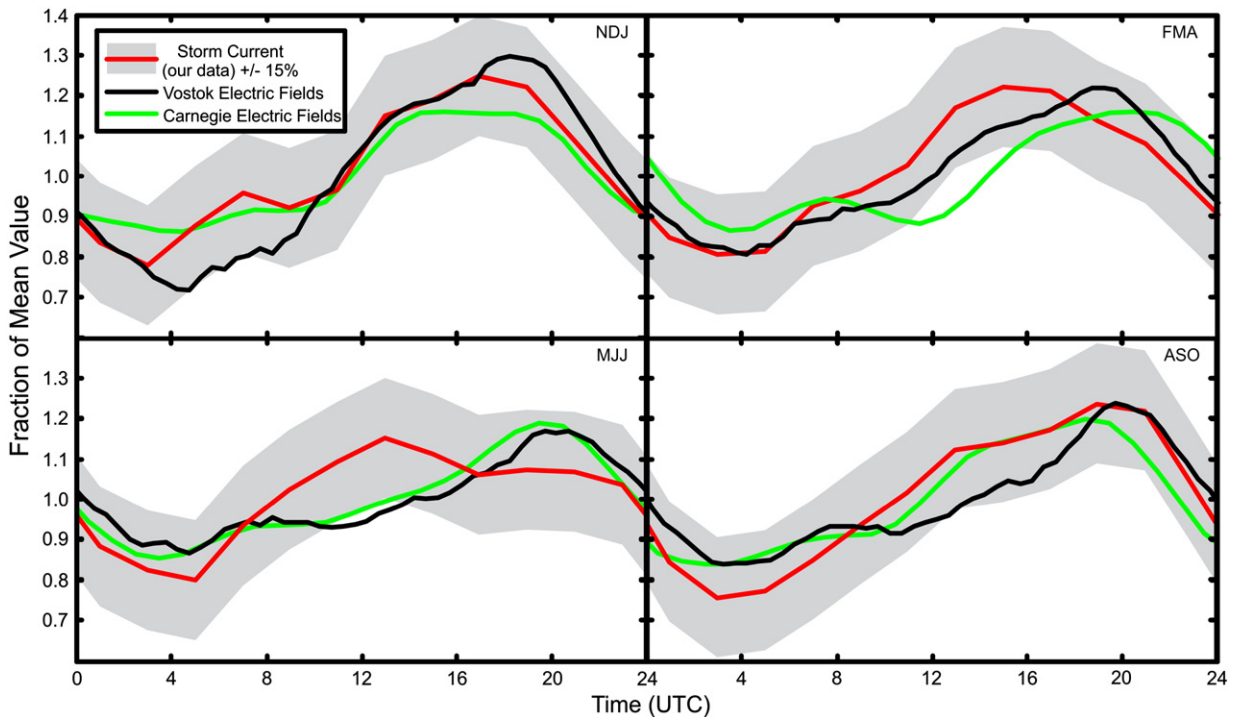
Fig. 14. Comparison of seasonal representations of the diurnal variation in the global electric circuit for November–January (NDJ, top left), February–April (FMA, top right), May–July (MJJ, bottom left), and August–October (ASO, bottom right). The black curves are the seasonal surface electric field from the Vostok station in Antarctica, the green curves are the seasonal diurnal variations of potential obtained during the Carnegie voyages, and the red curves, with a $\pm 15\%$ error bound shown in grey, are the seasonal total global currents from our combined satellite-airborne analyses of lightning and storm current. All the curves, taken in pairs, fall within 15% of each other (except for 2 short periods discussed in the text), which is on the order of the estimated error bar for each dataset.

spring lightning tends to exceed fall activity at most continental locations (but there are a few exceptions, e.g., central Canada, west coast of Mexico and United States).

5.2. Seasonal variations in total current

In our prior publication on the diurnal variation of current in the global electric circuit (Mach et al., 2011), we concluded that our results strongly supported on an annual basis that electrified storms with and without lightning are the sources for the fair weather electric field variations (i.e., the Carnegie Curve) as first hypothesized by Wilson (1921). In our analyses, satellite-derived global lightning statistics from the combined

Table 6
Root Mean Square (RMS) differences among the normalized seasonal diurnal variations of the global electric circuit from our diurnal current estimates (Current) diurnal electric field changes at Vostok, Antarctica (VOS), and diurnal potential gradient observations from the Carnegie voyages (Carnegie). The seasons are shifted one month from previous plots (i.e., November–December–January versus DJF, etc.) to enable direct intercomparison with the Carnegie results.

	VOS—Current%	Carnegie—Current%	Carnegie—VOS%
NDJ	7.4	4.0	9.1
FMA	5.9	11.6	7.3
MJJ	9.3	8.3	2.9
ASO	7.6	5.5	7.4

OTD/LIS dataset provided information on diurnal variations while high altitude aircraft cloud overflight measurements yielded knowledge of current output per storm as a function of flash rate for both thunderstorms and ESCs. Without using any "tuning," diurnal variation in the global electric circuit derived from combined satellite-aircraft data analysis fell mostly within 4% of the traditional Carnegie curve. The differences in current output between land and ocean storms accounted for most of the historically observed amplitude discrepancy between the Carnegie and lightning-only diurnal behavior, while including ESCs accounted for the rest. Mach et al. (2011) did point out that our overflight data may have had a slight selection bias toward lightning storms, with ESCs underestimated by a factor of 2 or 3. However, the inclusion of additional ESCs does not alter the fundamental conclusion.

A major objective of this paper was to extend the analysis of Mach et al. (2011) to shorter seasonal periods using expanded datasets of both storm overflights and orbital lightning data. In support of this, we compared our combined satellite-aircraft data analysis to two independent seasonal measures of the global electric circuit—one derived from the monthly mean diurnal electric field at Vostok, Antarctica (Burns et al., 2005) and the other from potential gradient observations obtained during the Carnegie voyages (Torreson et al., 1946). Our seasonal results, normalized to the mean, match the normalized Vostok and Carnegie observations to within 15%, which is about the size of the error terms in each individual measurement. Each curve differs from the others

in similar fashion and magnitude. Again, this "untuned" agreement quantitatively and strongly demonstrates how electrified storms generate the observed global electric circuit variations. The more "random" storm selection in the GRIP data set may have lowered slightly the ESC under sampling bias, but this remains a second order effect.

It is worth noting that by properly accounting for land–ocean current output differences and the current contribution from ESCs, land storms with lightning only account for half of the global current. Ocean storms, with higher current output per flash rate, contribute one third of the global current from lightning storms and one sixth from ESCs. Also, the flat diurnal behavior of ocean storms, coupled with its significant current contribution is a key factor in "damping" the much larger amplitude variation in global lightning rates as compared to the fair weather electric field variations found in the Carnegie curve and similar observations.

5.3. Final comments

We feel there is little doubt that the results presented in Mach et al. (2011) and in this paper establish that electrified storms are the source of the fair weather electric field and quantitatively account for their contributions. This had remained a scientific puzzle until now. Although not as directly quantitative, Liu et al. (2010) offered an alternate solution that also was strongly suggestive of this same conclusion. As one science problem is resolved, fascinating new questions arise. Some new questions raised by this work are (1) why are land and ocean storms so different in their electric current output per flash rate, including the zero flash rate ESCs and (2) why do land ESCs contribute so little current to the global circuit?

Acknowledgments

References

Bailey, J.C., Blakeslee, R.J., Buechler, D.E., Christian, H.J., 2007. Diurnal lightning distributions as observed by the Optical Transient Detector (OTD) and the Lightning Imaging Sensor (LIS). Proceedings of the 13th International Conf. on Atmos. Elec., Vol. II, pp. 657–660. Organized by the International Commission on Atmospheric Electricity (ICAE/IAMAS/IUGG): August 13-17, 2007, Beijing Friendship Hotel, China.

Bateman, M.G., Stewart, M.F., Blakeslee, R.J., Podgorny, S.J., Christian, H.J., Mach, D.M., Bailey, J.C., Daskar, D., 2007. A low-noise, microprocessor-controlled, internally digitizing rotating-vane electric field mill for airborne platforms. J. Atmos. Ocean. Tech. 24, 1245–1255 http://dx.doi.org/10.1175/JTECH2039.1.

Blakeslee, R.J., Christian, H.J., Vonnegut, B., 1989. Electrical measurements over thunderstorms. J. Geophys. Res. 94, 13135–13140.

Blakeslee, R.J., Driscoll, K.T., Buechler, D.E., Boccippio, D.J., Boeck, W.L., Christian, H.J., Goodman, S.J., Hall, J.M., Koshak, W.J., Mach, D.M., Stewart, M.F., 1999. Diurnal lightning distribution as observed by the Optical Transient Detector (OTD). 11th International Conf. on Atmos. Elec., Proceedings, NASA/CP–1999–209261, 742–745, Guntersville, Alabama, June 7–11, 1999.

Blakeslee, R.J., Mach, D.M., Desch, M.D., Goldberg, R.A., Farrell, W.M., Houser, J.G., 2002. The Altus Cumulus Electrification Study (ACES): a UAV-based science demonstration. AIAA's 1st Technical Conference and Workshop on Unmanned Aerospace Vehicles, Systems, Technologies, and Operations, AIAA-2002-3405, Portsmouth, VA, 20–23 May 2002.

Boccippio, D.J., Koshak, W., Blakeslee, R., Driscoll, K., Mach, D., Buechler, D., Boeck, W., Christian, H.J., Goodman, S.J., 2000a. The Optical Transient Detector (OTD): instrument characteristics and cross sensor validation. J. Atmos. Oceanic Technol. 17, 441–458 http://dx.doi.org/10.1175/1520-0426.

Boccippio, D.J., Goodman, S.J., Heckman, S., 2000b. Regional differences in tropical lightning distributions. J. Appl. Meteorol. 39, 2231–2248 http://dx.doi.org/10.1175/1520-0450.

Boccippio, D.J., Koshak, W.J., Blakeslee, R.J., 2002. Performance assessment of the optical transient detector and lightning imaging sensor. Part I: Predicted diurnal variability. J. Atmos. Oceanic Technol. 19, 1318–1332.

Braun, S.A., Kakar, R., Zipser, E., Heymsfield, G., Albers, C., Brown, S., Durden, S.L., Guimond, S., Halverson, J., Heymsfield, A., Ismail, S., Lambrigtsen, B., Miller, T., Tanelli, S., Thomas, J., Zawislak, J., 2012. NASA's Genesis and Rapid Intensification Processes (GRIP) field experiment. Bull. Am. Meteorol. Soc. http://dx.doi.org/10.1175/BAMS-D-11-00232.1.

Burns, G.B., Frank-Kamenetsky, A.V., Troshichev, O.A., Bering, E.A., Reddell, B.D., 2005. Interannual consistency of bi-monthly differences in annual variations of the ground-level, vertical electric field. J. Geophys. Res. 110 (D10106) http://dx.doi.org/10.1029/2004JD005469.

Cecil, D.J., Buechler, D.E., Blakeslee, R.J., 2014. Gridded lightning climatology from TRMM-LIS and OTD: dataset description. Atmos. Res. 135-136, 401–411 (this issue).

Christian, H.J., Driscoll, K.T., Goodman, S.J., Blakeslee, R.J., Mach, D.A., Buechler, D.E., 1996. The Optical Transient Detector (OTD). Proceedings of the 10th International Conference on Atmospheric Electricity; Osaka, Japan; June 10–14, 1996, pp. 368–371.

Christian, H.J., Blakeslee, R.J., Goodman, S.J., Mach, D.M., Stewart, M.F., Buechler, D.E., Koshak, W.J., Hall, J.M., Boeck, W.L., Driscoll, K.T., Boccippio, D.J., 1999. The lightning imaging sensor. Proc. 11th Int. Conf. on Atmospheric Electricity, Guntersville, AL, pp. 746–749.

Christian, H.J., Blakeslee, R.J., Boccippio, D.J., Boeck, W.L., Buechler, D.E., Driscoll, K.T., Goodman, S.J., Hall, J.M., Koshak, W.J., Mach, D.M., Stewart, M.F., 2003. Global frequency and distribution of lightning as observed from space by the Optical Transient Detector. J. Geophys. Res. 108, 4005 http://dx.doi.org/10.1029/2002JD002347.

Farrell, W.M., Goldberg, R.A., Blakeslee, R.J., Desch, M.D., Mach, D.M., 2006. Radiation impedance over a thunderstorm. Radio Sci. 41, RS3008 http://dx.doi.org/10.1029/2004RS003217.

Gringel, W., Rosen, J.M., Hofmann, D.J., 1986. Electrical structure from 0 to 30 kilometers. The Earth's Electrical Environment (Studies in Geophysics). National Academy Press, pp. 166–182.

Heymsfield, G.M., Halverson, J.B., Simpson, J., Tian, L., Bui, T.P., 2001. ER-2 Doppler radar investigations of the eyewall of hurricane Bonnie during the convection and moisture experiment-3. J. Appl. Meteorol. 40, 1310–1330.

Hood, R.E., Cecil, D.J., LaFontaine, F.J., Blakeslee, R.J., Mach, D.M., Heymsfield, G.M., Marks Jr., F.D., Zipser, E.J., Goodman, M., 2006. Classification of tropical oceanic precipitation using high-altitude aircraft microwave and electric field measurements. J. Atmos. Sci. 63, 218–233 http://dx.doi.org/10.1175/JAS3606.1.

Ivancic, W.D., Sullivan, D.V., 2010. Delivery of unmanned aerial vehicle DATA. presented at The 2010 Earth Science Technology Forum, Arlington, VA, June 22–24, 2010.

Ivancic, W.D., Stewart, D.E., Sullivan, D.V., Finch, P.E., 2011. An evaluation of protocols for UAV science applications. presented at The 2011 Earth Science Technology Forum, Pasadena, CA, June 21–23, 2011.

Koshak, W.J., Bergstrom, J.W., Stewart, M.F., Christian, H.J., Hall, J.M., Solakiewicz, R.J., 2000. Laboratory calibration of the Optical Transient Detector and the Lighting Imaging Sensor. J. Atmos. Oceanic Technol. 17, 905–915.

Kummerow, C., et al., 2000. The status of the Tropical Rainfall Measuring Mission (TRMM) after two years in orbit. J. Appl. Meteorol. 39, 1965–1982.

Kummerow, C., Barnes, W., Kozu, T., Shiue, J., Simpson, J., 1998. The tropical rainfall measuring mission (TRMM) sensor package. J. Atmos. Oceanic Technol. 15, 809–817.

Liu, C., Williams, E., Zipser, E.J., Burns, G., 2010. Diurnal variations of global thunderstorms and electrified shower clouds and their contribution to the global electrical circuit. J. Atmos. Sci. 67, 309–323 http://dx.doi.org/10.1175/2009JAS3248.1.

Mach, D.M., Blakeslee, R.J., Bailey, J.C., Farrell, W.M., Goldberg, R.A., Desch, M.D., Houser, J.G., 2005. Lightning optical pulse statistics from storm overflights during the Altus Cumulus Electrification Study. Atmos. Res. 76, 386–401 http://dx.doi.org/10.1016/j.atmosres.2004.11.039.

Mach, D.M., Blakeslee, R.J., Bateman, M.G., Bailey, J.C., 2009. Electric fields, conductivity, and estimated currents from aircraft overflights of electrified clouds. J. Geophys. Res. 114, D10204 http://dx.doi.org/10.1029/2008JD011495.

Mach, D.M., Blakeslee, R.J., Bateman, M.G., Bailey, J.C., 2010. Comparisons of total currents based on storm location, polarity, and flash rates derived from high altitude aircraft overflights. J. Geophys. Res. 115, D03201 http://dx.doi.org/10.1029/2009JD012240.

Mach, D.M., Blakeslee, R.J., Bateman, M.G., 2011. Global electric circuit implications of combined aircraft storm electric current measurements and satellite-based diurnal lightning statistics. J. Geophys. Res. 116, D05201 http://dx.doi.org/10.1029/2010JD014462.

Markson, R., 1976. Ionospheric potential variation obtained from aircraft measurements of potential gradient. J. Geophys. Res. 81, 1980–1990.

Markson, R., 1977. Airborne atmospheric electrical measurements of the variation of ionospheric potential and electrical structure in the exchange layer over the ocean. In: Dolezalek, H., Reiter, R. (Eds.), Electrical Processes in Atmospheres. Steinkopff, Darmstadt, p. 450.

Ogawa, T., Komatsu, M., 2009. Q-bursts from various distances on the Earth. Atmos. Res. 91, 538–545 http://dx.doi.org/10.1016/j.atmosres.2008.04.013.

Orville, R.E., Henderson, R.E., 1986. Global distribution of midnight lightning: September 1977 to August 1978. Mon. Wea. Rev. 114, 2640–2653 http://dx.doi.org/10.1175/1520-0493.

Orville, R.E., Huffines, G.R., Burrows, W.R., Cummins, K.L., 2011. The North American Lightning Detection Network (NALDN)—analysis of flash data: 2001–09. Mon. Wea. Rev. 139, 1305–1322 http://dx.doi.org/10.1175/2010MWR3452.1.

Roble, R.G., Tzur, I., 1986. The global atmospheric–electrical circuit. The Earth's Electrical Environment. Natl. Acad. Press, Washington, D. C.

Torreson, O.W., Parkinson, W.C., Gish, O.H., Wait, G.R., 1946. Ocean atmospheric electricity results, scientific results of Cruise VII of the Carnegie during 1928–1929, Publ. 568. Carnegie Inst, Washington, D.C.

U.S. Department of Commerce, National Oceanic and Atmospheric Administration, National Geophysical Data Center, 2006. 2-minute Gridded Global Relief Data (ETOPO2v2). http://www.ngdc.noaa.gov/mgg/fliers/06mgg01.html, 2007.

Virts, K.S., Wallace, J.M., Hutchins, M.L., Holzworth, R.H., submitted for publication. A new ground-base, hourly global lightning climatology. Bull. Am. Meteorol. Soc.

Wallace, J.M., 1975. Diurnal variations in precipitation and thunderstorm frequency over the conterminous United States. Mon. Wea. Rev. 103, 406–419 http://dx.doi.org/10.1175/1520-0493(1975)103<0406:DVIPAT>2.0.CO;2.

Whipple, F.J.W., 1929. On the association of the diurnal variation of electric potential gradient in fine weather with the distribution of thunderstorms over the globe. Q. J. R. Meteorolog. Soc. 55, 1–17.

Whipple, F.J.W., Scrase, F.J., 1936. Point-discharge in the electric field of the Earth. Geophys. Mem. VII (68), 1–20.

Williams, E.R., 2009. The global electrical circuit: a review. Atmos. Res. 91 (2), 140–152 http://dx.doi.org/10.1016/j.atmosres.2008.05.018.

Williams, E.R., Heckman, S.J., 1993. The local diurnal variation of cloud electrification and the global diurnal variation of negative charge on the earth. J. Geophys. Res. 98, 5221–5234.

Williams, E., Rosenfeld, D., Madden, N., Gerlach, J., Gears, N., Atkinson, L., Dunnemann, N., Frostrom, G., Antonio, M., Biazon, B., Camargo, R., Franca, H., Gomes, A., Lima, M., Machado, R., Manhaes, S., Nachtigall, L., Piva, H., Quintiliano, W., Machado, L., Artaxo, P., Roberts, G., Renno, N., Blakeslee, R., Bailey, J., Boccippio, D., Betts, A., Wolff, D., Roy, B., Halverson, J., Rickenbach, T., Fuentes, J., Avelino, E., 2002. Contrasting convective regimes over the Amazon: implications for cloud electrification. J. Geophys. Res. 107 http://dx.doi.org/10.1029/2001JD000380.

Wilson, C.T.R., 1921. Investigations on lightning discharges and on the electric field of thunderstorms. Philos. Trans. R. Soc. Lond. A 221, 73–115.

Zipser, E.J., Cecil, D.J., Liu, C., Nesbitt, S.W., Yorty, D.P., 2006. Where are the most intense thunderstorms on earth? Bull. Am. Meteorol. Soc. 87, 1057–1071.